JOURNAL OF GEOPHYSICAL RESEARCH, VOL. 105, NO. B9, PAGES 21,745–21,759, SEPTEMBER 10, 2000

Mode of Cenozoic east-west extension in Tibet suggesting a common origin of rifts in Asia during the Indo-Asian collision

An Yin

Department of Earth and Space Sciences and Institute of Geophysics and Planetary Physics
University of California, Los Angeles

Abstract. Cenozoic rifts in Tibet were traditionally interpreted as a result of topographic collapse of the Tibetan Plateau, reaching the maximum elevation that can be supported by its mechanical strength. Recent studies have emphasized possible similarities between rifting in Tibet and extension in the Basin and Range of the western United States. However, when examined in detail, one finds that spacing of long (>100 km) rifts in Tibet (~100-300 km) is significantly greater than that in the Basin and Range (~20-40 km). From south to north, rift spacing decreases systematically: from 191±67 km in the Himalaya south of the Indus-Yalu suture to 146±34 km in south Tibet between the Indus-Yalu and Bangong-Nujiang sutures and farther north to 101±31 km in central Tibet between the Bangong-Nujiang and Jinsha sutures. Instability analysis suggests that the mantle lithosphere must have been involved in east-west Tibetan extension. Specifically, the widely spaced rifts in The Himalaya and Tibet may have been related to the presence of a relatively light crust (density <~2.90 g cm^{-3}) and a strong mantle lithosphere (~ 40 km thick and a factor of 5 stronger than the upper crust). The observed systematic decrease in rift spacing can be explained by the known decrease in the crustal thickness in Tibet, from ~70-80 km in The Himalaya in the south to ~50-55 km in central Tibet in the north. A regional comparison of rifts in east Asia suggests that both the involvement of the mantle lithosphere and the age of rift initiation are similar for Tibetan rifts, the Baikal rift, and the Shanxi graben. This implies that topographic collapse or a convective event in the mantle cannot be the sole cause for the development of the Tibetan rifts. A regional boundary condition applied throughout east Asia must be required.

1. Introduction

To understand the formation of the Tibetan Plateau, we need to know whether deformation in the crust and the mantle lithosphere shares the same kinematics during the Indo-Asian collision [e.g., *Holt*, 2000]. Two hypotheses have been proposed in this regard. The first hypothesis considers deformation of the lithosphere to be uniform in a vertical profile; therefore surface deformation represents the same strain history and distribution in the entire lithosphere [*Tapponnier et al.*, 1982; *England and Houseman*, 1986]. In contrast, the second hypothesis argues that the existence of a weak lower crust for the continental lithosphere indicates that the upper crust and the mantle lithosphere may have experienced different kinematic patterns and strain histories during the Indo-Asian collision, which permits horizontal injection and diffusion of ductile lower crustal materials in and out of Tibet [*Zhao and Morgan*, 1987; *Bird*, 1991; *Masek et al.*, 1994; *Royden*, 1996] and the development of subhorizontal detachment faults in the middle and lower crust [*Burchfiel et al.*, 1989; *Zhao et al.*, 1993; *Hauck et al.*, 1998]. A test of the two contrasting models would require tracking surface deformation vertically downward to the lower crust and the mantle lithosphere. On the basis of observations from wide-angle seismic reflection profiles, *Hirn et al.* [1984] suggested that the Moho is offset beneath The Himalaya by major thrust faults, implying that the mode of compressional deformation in the crust can be extrapolated into the upper mantle. *Molnar and Chen* [1983] showed that active east-west extension in southern Tibet is expressed by earthquake faulting in the upper crust and the upper mantle despite the presence of a weak and aseismic lower crust [*Chen and Molnar*, 1983]. Recent fault plane solutions and focal depth determination further suggest that brittle east-west extension in the upper crust and the mantle shares the same mode of deformation directly beneath north-south trending rifts in The Himalaya [*Chen and Kao*, 1996]. Although calculating focal depths without local stations such as in Tibet may render large uncertainties [*Zhao and Helmberger*, 1991], careful waveform modeling of deep seismic events (70-100 km) confirms the occurrence of normal faulting events in the mantle beneath southern Tibet and The Himalaya [e.g., *Chen and Kao*, 1996] (Plate 1). Because lithospheric deformation is widespread in Tibet [*Molnar and Lyon-Caen*, 1989; *Armijo et al.*, 1989], the rate of slip on individual structures may be relatively low. Thus the interseismic intervals for occurrence of large earthquakes in the upper mantle may be as long as several thousands of years. This presents difficulties in evaluating whether seismicity in the upper mantle is restricted only to southern Tibet or regionally significant for the entire Tibetan Plateau.

Recent interpretations of seismic reflection and refraction data suggest that structures associated with north-south trending rifts may be restricted only to the upper crust [*Cogan et al.*, 1998] because of the presence of a partially molten lower Tibetan crust [*Nelson et al.*, 1996]. This interpretation does not preclude the mantle lithosphere to have experienced necking (i.e., localized thinning below the crustal rift) during the extension, with the ductile lower crust acting as the accommodation zone between the brittle upper crust and the mantle lithosphere. Because crustal reflection seismology could not resolve detailed structures in the lithosphere directly beneath the rifts, an independent means is needed to evaluate how the mantle lithosphere has participated in late Cenozoic Tibetan extension. In this paper, I first summarize the current knowledge of Cenozoic north-south trending rifts in Tibet, which as shown below is rather poorly constrained. This is followed by a systematic analysis of Tibetan rift spacing based on a mechanical model that links spacing to mechanical properties of the lithosphere. The result of this analysis is then used to compare mode and timing of Cenozoic rift development in both Tibet and east Asia (e.g., Baikal rift and Shanxi graben) (Figure 1).

Paper number 2000JB900168.
0148-0227/00/2000JB900168$09.00

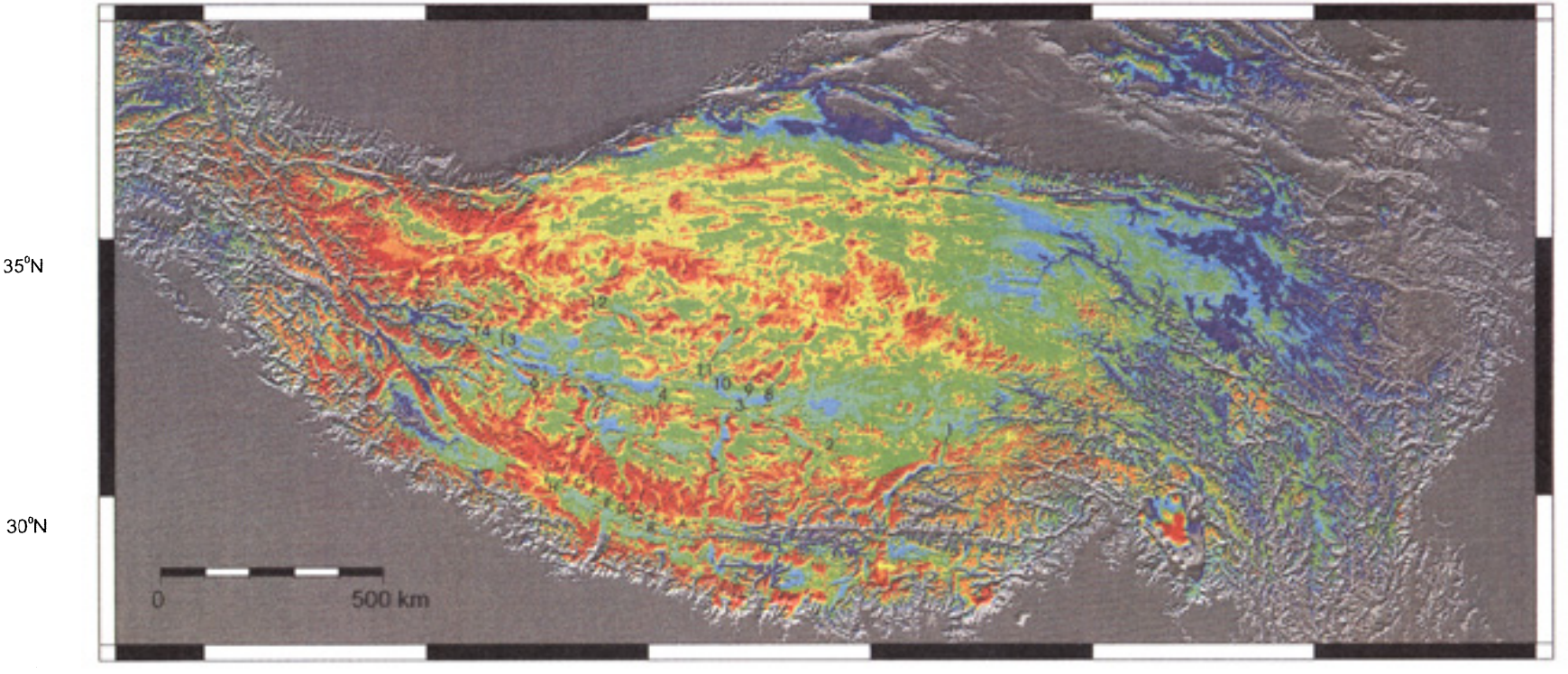

Plate 1a. Digital topographic map of Tibet. Numbers 1 to 7 indicate the presence of seven major rifts in south Tibet, numbers 8 to 16 are the most prominent rifts in central Tibet, and letters A to I indicate the locations of nine short and closely spaced rifts in southernmost Tibet. The overall rift distribution in the Himalaya and Tibet is shown in Plate 1b.

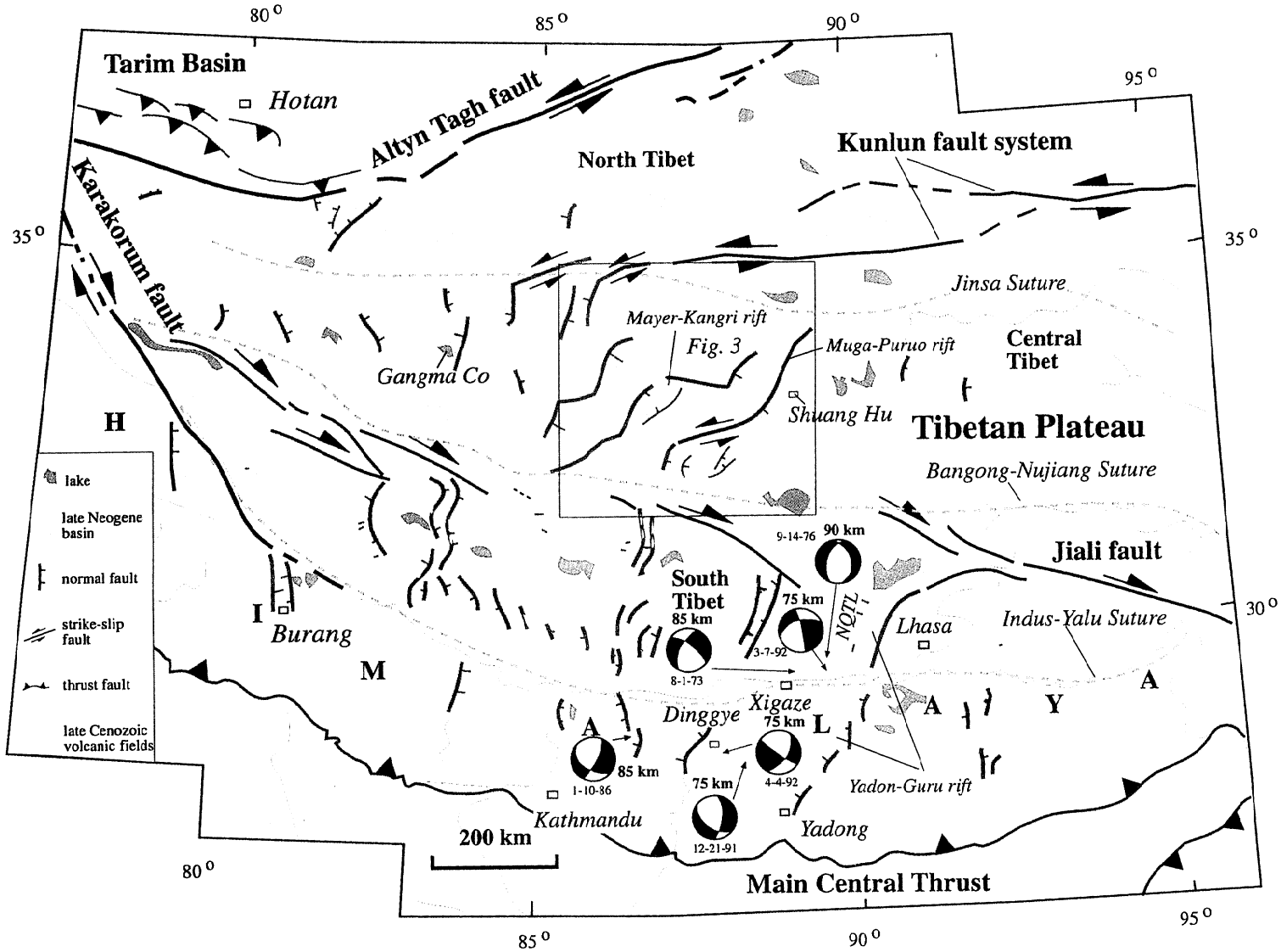

Plate 1b. Tectonic map of north-south trending rifts in Tibet, modified after *Armijo et al.* [1986], and location of Figure 2. Three major sutures divide Tibet and The Himalaya into four broad east-west trending zones. From south to north, they are (1) Himalaya, (2) south Tibet, (3) central Tibet, and (4) north Tibet. Note that the rifts in central Tibet merge with northeast trending left-slip faults at their north and the south ends. This pattern is a mirror image of the rifts and right-slip faults in south Tibet. Earthquakes at mantle depths with normal fault plane solutions are also shown. Data adapted from *Chen and Kao* [1996]. NQTL, Nyainquentanghla.

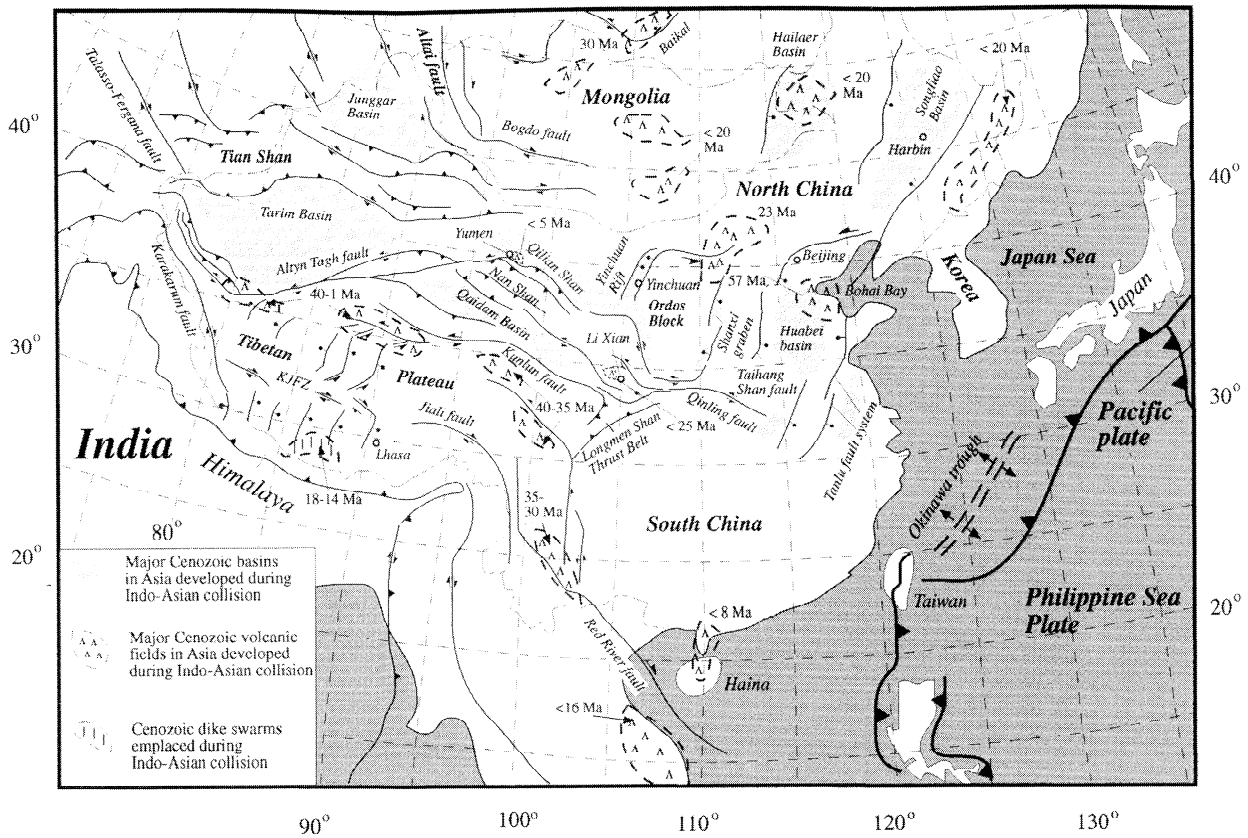

Figure 1. Active tectonic map of Asia, showing major Cenozoic fault systems, basins, and volcanic fields. Note that the active Kunlun fault marks approximately the northern boundary of north-south trending rifts in Tibet. Its western end terminates into a series of north-south trending rifts in Tibet, whereas its eastern end merges with the western end of the Qinling fault [*Peltzer et al.*, 1985] that is in turn linked with the north-south trending Shanxi graben in north China [*Zhang et al.*, 1998]. This configuration suggests that active rifting in Tibet is kinematically linked with active extension in north China. The right-slip Karakorum-Jiali fault zone (KJFZ) of *Armijo et al.* [1986] consists of (1) the Karakorum fault in west Tibet, (2) a series of right-slip faults linking north-south trending rifts in central Tibet, and (3) the Jiali fault in east Tibet. Major Cenozoic volcanic fields in Asia and their initiation ages are also shown. Source of data for distribution of Cenozoic igneous rocks are for north China, *Wang* [1982] and *Ye et al.* [1987]; central and east Tibet, *Pan et al.* [1990] and *Chung et al.* [1998]; northwestern corner of Tibet near Yumen, *Pan et al.* [1990]; northeastern corner of Tibet near Li Xian, *Yu* [1991]; Baikal region, *Kiselev* [1987]; south central Tibet, *Yin et al.* [1994]; Mongolia, *Traynor and Sladen* [1995]; and Indochina, *Lee et al.* [1998].

2. Geologic Setting of North-South Trending Rifts in Tibet

Since the initial recognition of active north-south trending rifts in Tibet [*Tapponnier and Molnar*, 1977; *Molnar and Tapponnier*, 1978; *Ni and York*, 1978], our knowledge of these structures has greatly improved. This may be attributed to several detailed field investigations in southern Tibet [*Tapponnier et al.*, 1981; *Armijo et al.*, 1986, 1989; *Mercier et al.*, 1987; *Burchfiel et al.*, 1991], improved quality of Landsat imagery [*Rothery and Drury*, 1984], and availability of seismic reflection and refraction data in south Tibet [*Cogan et al.*, 1998]. Because the initiation age of east-west extension in Tibet may represent the time when the plateau reached its present elevation [*Molnar and Tapponnier*, 1978; *England and Houseman*, 1989], which in turn may have been related to intensification of the Asian monsoon [*Harrison et al.*, 1992; *Molnar et al.*, 1993], efforts have been made to constrain the timing of extension. In the Nyainquentanghla region (Plate 1b), the age of onset of east-west extension is constrained to be 8±1 Ma [*Harrison et al.*, 1995; *Pan and Kidd*, 1993]. The age of extension in southernmost Tibet near Xigaze and the central Himalaya (Plate 1) was estimated by dating north-south trending dikes as 18±1 Ma [*Yin et al.*, 1994] and ~14 Ma [*Coleman and Hodges*, 1995], respectively. Whether dike emplacement represents a regional stress state or is significant only at a local scale has been debated [e.g., *Harrison et al.*, 1995], as they are not seen as widespread features associated with active Tibetan rifts.

The studies of north Tibetan rifts have been mostly based on fault plane solutions of earthquakes and interpretations of Landsat images [*Molnar and Lyon-Caen*, 1989; *Rothery and Drury*, 1984; *Armijo et al.*, 1986]. An exception is the geologic mapping conducted in north central Tibet near Gangma Co and Shuang Hu (Plate 1 and Figure 2), which shows the presence of major active normal fault systems with 4-8 km displacements [*Yin et al.*, 1999]. Kinematic analysis of these active faults suggests that northeast striking faults in the region are left-slip [*Yin et al.*, 1999; *Blisniuk et al.*, 1998], which are linked with north-south trending normal faults (Figure 2). The initiation age of rifts in north Tibet is estimated to have occurred in the past 3-4 Myr [*Yin et al.*, 1999].

3. Mechanisms for the Development of Tibetan Rifts

Traditionally, late Cenozoic east-west extension of Tibet was related to gravitational spreading of the overthickened crust [*Molnar and Tapponnier*, 1978; *Dewey*, 1988]. More recently, *England and Houseman* [1989] attributed extension to convective removal of the lower mantle lithosphere. Other workers, however, emphasized spatial restriction of east-west extension in southern Tibet [*Tapponnier et al.*, 1981; *Armijo et al.*, 1986; *Ratschbacher et al.*, 1994] and argued that rift formation was due to local boundary conditions such as oblique convergence between India and Asia or radially outward expansion of the Himalayan arc over the rigid Indian continent during the Indo-Asian collision [*Seeber and Arm-*

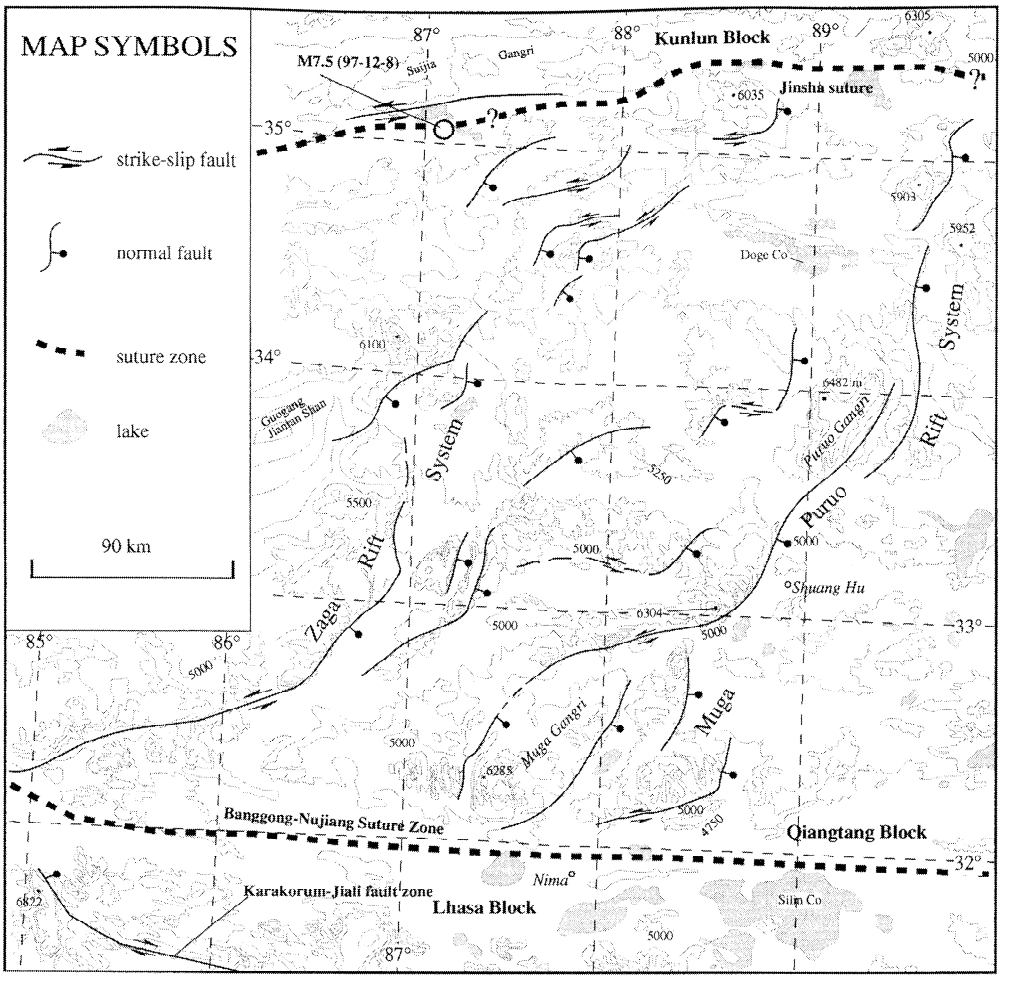

Figure 2. A sketch map showing major north-south trending normal faults in central Tibet. The topographic contours are based on the map of *Liao* [1990]. See Plate 1b for location. The interpretation of the normal and strike-slip faults and their kinematics is based on the works of *Liao* [1990] and *Blisniuk et al.* [1998], and the observations of *Yin et al.* [1999]. The Muga Puruo Rift system extends ~350 km along and terminates near the Jinsha suture to the north and the Bangong-Nujiang suture to the south. The central segment of the rift system near Shuang Hu is mapped in detail by *Yin et al.* [1999]. Note that the generally north-south trending normal faults merge with east-west and northeast-southwest trending left-slip faults. This is in contrast to the fault pattern in south Tibet, where north-south trending normal faults merge with northwest-southeast trending right-slip faults.

bruster, 1984; *Klootwijk et al.*, 1985; *Armijo et al.*, 1986, 1989; *Molnar and Lyon-Caen*, 1989; *Ratschbacher et al.*, 1994; *McCaffery and Nabelek*, 1998; *Seeber and Pecher*, 1998]. It is possible that the processes of gravitational spreading, a convective event in the mantle, and southward bulge of the Himalayan arc all contributed to east-west extension. However, the disagreements reflect the fact that we know little about the timing of initiation as well as the vertical extent of Tibetan extension. Several questions must be addressed to differentiate the above models: (1) Does the origin of Cenozoic normal faults in Tibet differ from those outside the plateau in eastern Asia (e.g., Lake Baikal, Shanxi graben)? (2) What are the characteristic geologic histories and initiation age of normal faults in and outside the plateau. (3) Is east-west extension restricted only to the upper crust or does it extend into the mantle lithosphere?

4. Rift Spacing in Tibet

4.1. Spatial Variation

Molnar and Tapponnier [1978] were the first to point out the remarkably uniform spacing of north-south trending rifts in southern Tibet (Plate 1a). *Armijo et al.* [1986] noted a decrease in rift spacing from south to north across the Tibetan Plateau. Using *Armijo et al.'s* [1986] compilation aided with recent field observations in north Tibet [*Kapp et al.*, 1997, 1998; *Yin et al.*, 1998, 1999] (Plate 1 and Figure 2), the distribution of Tibetan rift spacing is plotted in Figure 3. In the following, I define rifts as linear morphologic features that are bounded by active normal faults with magnitudes of slip greater than a few kilometers. The related topographic relieves across the rift zones are at least several hundreds of meters. Because active rifts in Tibet are expressed by narrow topographic depression filled by Cenozoic sediments (Plate 1), I define rift spacing as a distance between the centers of two nearby rift basins perpendicular to the strike of the rifts. The length of a rift can be defined by the length of a continuous topographic depression on map view. Using the above definitions, four distinctive east-west trending belts are recognized based on spacing and length of rifts (Plate 1): (1) the Himalayan region south of the Indus-Zangbu suture, (2) the southern Tibetan region between the Indus-Zangbu and the Bangong-Nujiang sutures, (3) the central Tibetan region between the Bangong-Nujiang and the Jinsha sutures, and (4) the northern Tibetan region north of the Jinsha suture.

The average rift spacing in The Himalaya is ~191 km with a large deviation ($1\sigma = \pm 67$ km, where σ is standard deviation). The length of the rifts ranges from ~120 to ~300 km. Although individual normal faults can not be traced directly across the Indus-Zangbu suture, the general trend of some rifts (e.g., the Yadong-Gulu rift) may be extended from The Hima-

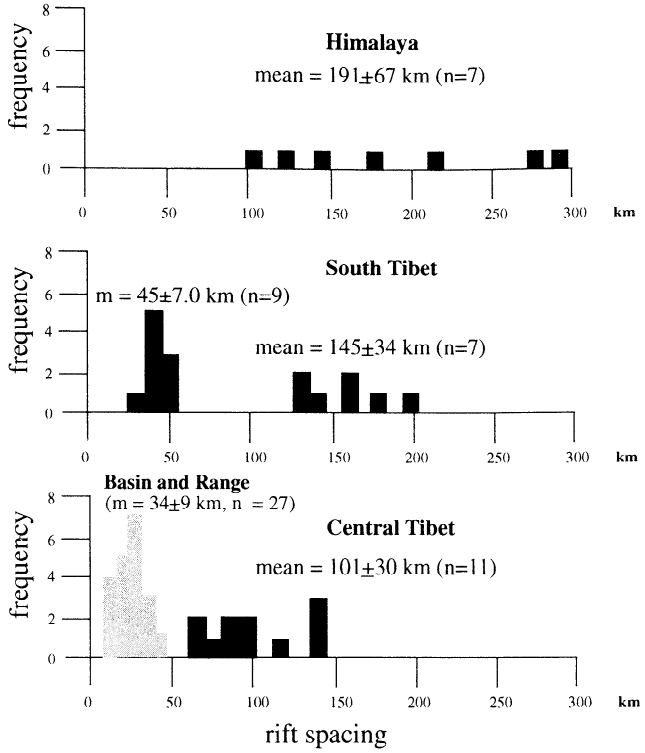

Figure 3. Histograms showing rift spacing in The Himalaya, south Tibet, and central Tibet. Typical spacing of active normal faults in the Basin and Range of the western United States [*Fletcher and Hallet*, 1983] is also shown for comparison. Although the average spacing of the Tibetan rifts decreases from south to north, the spread is quite significant, particularly for those in The Himalaya. The rift spacing in south Tibet is bimodal: one group shares an average rift spacing of ~45 km, and the other group has an average rift spacing of ~145 km. In all cases, the rift spacing in The Himalaya and Tibet is significantly greater than that for the Basin and Range of the western United States.

layas into Tibet (Plate 1). Despite the large deviation in rift spacing in The Himalaya, the distance between rifts in the region varies systematically in space. The more widely spaced rifts (260-300 km) lie near the western and eastern Himalaya syntaxes, whereas the more closely spaced rifts (110-150 km) are located in the central Himalaya.

Because southern Tibetan rifts have the strongest morphological expression [*Fielding et al.*, 1994] (Plate 1a), they have become the focus of most studies [e.g., *Armijo et al.*, 1986, 1989; *Ratschbacher et al.*, 1994; *Harrison et al.*, 1995]. In general, these rifts are longer (~300 km) and more continuous for both individual faults and overall rift systems than those in The Himalayas [*Armijo et al.*, 1986]. Two populations of rifts in this region can be clearly defined based on their spacing and along-strike length. The first are the well-known seven major rifts [*Armijo et al.*, 1986] (labeled as 1-7 in Plate 1a), which are several hundreds of kilometers long and are spaced at ~146±34 km (Figure 3). The second group consists of nine short rifts (<130 km long, labeled as A-I in Plate 1a), all in south central Tibet and next to one another (Plate 1). They are spaced at 46±7 km. These short rifts bound a series of north-south trending, narrow lakes such as Dajia Co and Jiesha Co (Plate 1).

Central Tibetan rifts are less prominent in their morphologic expressions [*Fielding et al.*, 1994] (Plate 1a), possibly due to the fact that the stream systems are internally drained [*Liao*, 1990] which suppresses topographic relief. The length of the rifts are highly variable and less continuous than those in southern Tibet [*Armijo et al.*, 1986]. The average rift spacing in central Tibet is ~101±31 km (Figures 2 and 3), significantly shorter than the long rifts in south Tibet and The Himalaya.

Whether or not late Cenozoic east-west extension has developed in north Tibet is not clear because no detailed surface geologic investigations have been conducted in the region. Although fault plane solutions of earthquakes show that the region undergoes both east-west extension and ENE and NW trending strike-slip faulting [*Molnar and Lyon-Caen*, 1989], morphologically, the inferred north-south trending extensional structures are poorly expressed [*Liao*, 1990; *Fielding et al.*, 1994] (Plate 1a).

The above analysis shows that the average spacing of the Himalayan-Tibetan rifts decreases northward, as noted by *Armijo et al.* [1986]. In particular, the decrease in rift spacing appears to occur abruptly across major sutures. On average, a decrease of ~50 km in rift spacing occurs from south to north across every suture between The Himalaya and north Tibet (Plate 1 and Figure 3), implying that the mechanical properties of individual Tibetan blocks are quite different from one another. This difference may have been directly controlled by the geologic history of Tibet prior to the Indo-Asian collision [*Allegre et al.*, 1984; *Dewey et al.*, 1988; *Yin and Nie*, 1996; *Murphy et al.*, 1997; *Yin et al.*, 1998; *Yin and Harrison*, 2000].

4.2. Comparison Between Tibetan Rifting and Basin-Range Extension: A Paradox

An analysis of digital topography across rifts in Tibet by *Masek et al.* [1994] shows that topographic highs occur along the rift flanks. These features were interpreted as rift shoulders related to flexural uplift caused by normal faulting. Modeling of the topographic profiles across the uplifts assuming an elastic upper crust on top of a Newtonian viscous lower crust indicates that the average effective elastic thickness of the Tibetan upper crust is ~6-7 km [*Masek et al.*, 1994]. A similar analysis applied by *Masek et al.* [1994] to the topography of the Basin and Range yields an average elastic thickness of 8-10 km for its upper crust.

Because the elastic thickness of the Tibetan Plateau and the Basin and Range is similar, one would expect that active extension should be expressed in a similar way. The active normal faults in the Basin and Range are spaced rather evenly [*Stewart*, 1971], at 34±9 km [*Fletcher and Hallet* , 1983] (Figure 3). This rift spacing can be explained by the presence of a strong plastic upper crust without the involvement of the upper mantle lithosphere [*Fletcher and Hallet*, 1983]. If Tibetan extension occurred under a similar condition, one would expect that the average spacing of major rifts in Tibet should be similar to that of the Basin and Range. Indeed, the rift spacing in the Basin and Range is similar to that of several short rifts in south central southern Tibet (Plate 1). However, when it is compared with the through going rifts that extend across both south Tibet and The Himalaya, rift spacing in the Basin and Range is only about 1/4 to 1/8 of those estimated in The Himalaya and Tibet. The similarities in rift morphology and elastic thickness, but a drastic difference in rift spacing between Tibet and the western United States, suggest that both boundary conditions and mechanical properties of the two extensional systems must be quite different [cf. *Nelson et al.*, 1996].

5. Mechanics of Tibetan Rift Spacing

In order to understand the dynamic conditions for the development of north-south trending Tibetan rift systems and their differences from those for the normal faults in the Basin and Range, rift spacing is used as a proxy for exploring rheological structures of the lithosphere. Although mechanics of evenly spaced folds are well understood [e.g., *Biot*, 1961; *Fletcher*, 1974], mechanisms that control instability and spacing of extensional structures (e.g., mullions and boundinages) had not been explicitly explained until the development of the infinitesimal instability theory of *Smith* [1975] for a Newtonian fluid and later for generalized non-

Newtonian fluids [*Smith*, 1977]. The fundamental physics of the theory is that in a mechanically stratified system the strength contrast between neighboring layers can produce a sharp pressure jump across the interface under uniform extension. Because the interfaces of the mechanical layers in reality are not perfect planes but irregular surfaces, under a small disturbance the pressure discontinuity across the interface can lead to mechanical instability expressed by a run-away growth of the preexisting irregularities.

Several advances have been made since *Smith*'s [1975] first formulation of the problem. A noticeable improvement of the theory was the addition of gravitational force by *Fletcher and Hallet* [1983]. This allows expansion of the theory from explaining mesoscopic folds and mullions (<1 km in dimension) to lithospheric scale tectonic problems [*Ricard and Froidevaux*, 1986; *Zuber et al.*, 1986; *Bassi and Bonnin*, 1988; *Martinod and Davy*, 1992].

In the *Smith* [1975] theory of extensional instability, deformation is assumed to be plane strain. This is probably a good approximation for Tibet in the past 15-20 Myr, as no east-west trending Neogene thrusts have been found. Another possible concern of the theory of *Smith* [1975] is that it deals with initiation of extension under infinitesimal strain. However, both scale-model experiments and numerical simulations demonstrate that the predictions of the theory can be reasonably extrapolated to finite amplitudes of folds and rifts [*Chapple*, 1968; *Mancktelow and Abbassi*, 1992; *Martinod and Davy*, 1994; *Zuber and Pamentier*, 1996; *Benes and Davy*, 1996].

5.1. Basic Equations

A four-layer mechanical system is considered under plane strain deformation (Figure 4). Owing to irregular surface topography and variations of composition and thermal gradients, the top surface and the contacts between the mechanical layers of the lithosphere and asthenosphere may not be perfectly planar. As the magnitude of vertical variation departing from perfectly planar interfaces between layers is likely small (<1-2 km) compared to the horizontal dimension of the mechanical system (>800 km for the extended part of Tibet), the total extensional deformation may be partitioned into two parts: (1) the basic flow, which is derived when treating all the contacts as planes, and (2) the perturbed flow, which is induced by small-amplitude topography at the boundaries of the mechanical layers. The total stress and strain rate for the combined flow may be written as

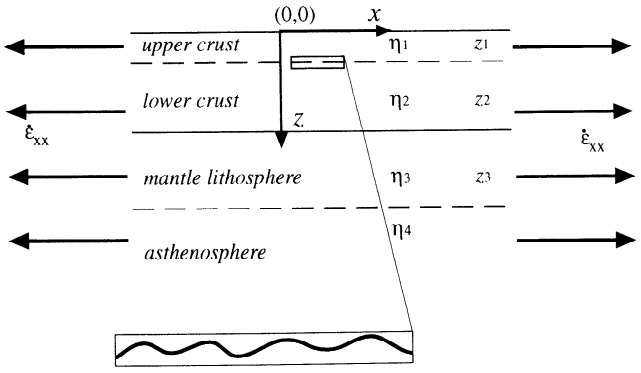

Figure 4. The model system and parameters used in calculation: z_1, z_2, and z_3 are thickness of the upper crust, the lower crust, and the mantle lithosphere, respectively; η_1, η_2, η_3, and η_4 are effective viscosity of the upper crust, the lower crust, the mantle lithosphere, and the asthenosphere, respectively; and $\dot{\varepsilon}_{xx}$ is the horizontal strain rate. For all the calculations, $\dot{\varepsilon}_{xx}$ is assumed to be 10^{-15} s^{-1}.

$$\sigma_{ij} = \bar{\sigma}_{ij} + \tilde{\sigma}_{ij},$$

and

$$\dot{\varepsilon}_{ij} = \bar{\dot{\varepsilon}}_{ij} + \tilde{\dot{\varepsilon}}_{ij},$$

where $\bar{\sigma}_{ij}$, $\tilde{\sigma}_{ij}$, $\bar{\dot{\varepsilon}}_{ij}$, and $\tilde{\dot{\varepsilon}}_{ij}$ represent stress and strain rate in the basic flow and the perturbed flow, respectively.

5.1.1. Basic flow. The formulation of the problem outlined below follows that developed by *Smith* [1975, 1977], *Fletcher and Hallet* [1983], and *Bassi and Bonnin* [1988]. First, we consider pure shear deformation under horizontal extension for the basic flow. Its strain rate tensor may be written as

$$\bar{\dot{\varepsilon}}_{ij} = \begin{pmatrix} \bar{\dot{\varepsilon}}_{xx} & 0 \\ 0 & \bar{\dot{\varepsilon}}_{zz} \end{pmatrix} = \begin{pmatrix} \dfrac{\partial \bar{u}}{\partial x} & 0 \\ 0 & \dfrac{\partial \bar{w}}{\partial z} \end{pmatrix}, \tag{1}$$

where $\dot{\varepsilon}_{xx}$ and $\dot{\varepsilon}_{yy}$ are horizontal and vertical extension rate components, and $\bar{u}$ and $\bar{w}$ are the horizontal and vertical velocity components, respectively. The condition of incompressibility requires that

$$\bar{\dot{\varepsilon}}_{xx} + \bar{\dot{\varepsilon}}_{zz} = \frac{\partial \bar{u}}{\partial x} + \frac{\partial \bar{w}}{\partial z} = 0 . \tag{2}$$

The relationship between stress and strain rate follows the power law

$$\bar{\sigma}_{ij} = 2\eta \bar{\dot{\varepsilon}}_{ij} - \bar{p}\delta_{ij} , \tag{3}$$

where $\bar{\sigma}_{ij}$ is the stress tensor, $\bar{p}$ is the pressure for the basic flow, and η is the effective viscosity for the basic flow as

$$2\eta = B^{-1} \exp(Q/RT) \bar{J}_2^{(1-n)/2} , \tag{4}$$

where B, Q, and n are material constants, R is the gas constant, and

$$\bar{J}_2 = 1/4(\bar{\sigma}_{xx} - \bar{\sigma}_{zz})^2$$

is the second invariant of the deviatoric stress tensor defined as

$$\Delta_{ij} = \bar{\sigma}_{ij} + \bar{p}\delta_{ij} .$$

For pure shear deformation (Figure 4), $\bar{\sigma}_{xz} = 0$. From (3) and

$$\bar{J}_2 = \frac{1}{4}(\bar{\sigma}_{xx} - \bar{\sigma}_{zz})^2 ,$$

we obtain

$$\bar{\sigma}_{xx} - \bar{\sigma}_{zz} = 4\eta \bar{\dot{\varepsilon}}_{ij} ,$$

and

$$\bar{J}_2 = 4\eta^2 \bar{\dot{\varepsilon}}_{ij}^2 .$$

This leads to the relationship between the effective viscosity and the horizontal extension rate

$$\eta = \frac{1}{2}\bar{\dot{\varepsilon}}_{xx}^{(1-n)/n} B^{-1/n} \exp(Q/nRT) . \quad (5)$$

As pointed out by *Fletcher and Hallet* [1983] and *Bassi and Bonnin* [1988], when n approaches infinity, the relationship shown in (3) is a good approximation for a perfect plastic material obeying the Von Mises criterion. That is,

$$\bar{J} = \tau_y^2 ,$$

where

$$\tau_y^2 = 2\eta \bar{\dot{\varepsilon}}_{xx}$$

is the yield stress for plastic deformation. For the viscous lower crust and the ductile asthenosphere the viscosity decreases exponentially with depth as the temperature increases [*Brace and Kohlstedt*, 1980; *Fletcher and Hallet*, 1983] such as $\eta = \eta_0 \exp(\gamma z)$, where η_0 and γ are related to both the material constants in (5) and the vertical temperature variation, $T = T(z)$. For layers with uniform viscosity, it requires $\gamma = 0$ and $\eta = \eta_0$. The average viscosity may be estimated by integrating $\eta(z)$ over each layer divided by the layer thickness, that is,

$$\eta_{ave} = \frac{1}{z_t}\int_0^{z_t} \eta(z) dz .$$

This allows the use of a constant viscosity for each mechanical layer when dealing with basic flow.

Zuber et al. [1986] showed that whether viscosity is constant or decreases exponentially with depth makes little difference in predicting dominant wavelengths for the initiation of extensional instability. In contrast, *Bassi and Bonnin* [1988] argued that the continental lithosphere with a strength profile constructed by *Brace and Kohlstedt* [1980] under uniform extension is always stable. The latter is drastically different from the conclusions reached by *Fletcher and Hallet* [1983] and *Zuber et al.* [1986]. The apparent difference in the results of *Zuber et al.* [1986] and *Bassi and Bonnin* [1988] could be explained by the choice of different model parameters, as pointed out by *Bassi and Bonnin* [1988]. Because the thermal structure and thus the rheological profile in The Himalaya and Tibet are highly uncertain, a simpler approach by *Zuber et al.*[1986] and *Ricard and Froidevaux* [1986] is adopted here, which assumes uniform viscosity for each mechanical layer in the model. The absolute value of the viscosity is implied by the assumed strain rate and the assume stress magnitude in the particular experiments that follow.

5.1.2. Perturbed flow. For the perturbed flow we obtained the relationship between stress and strain rate by substituting

$$\sigma_{ij} = \bar{\sigma}_{ij} + \tilde{\sigma}_{ij}$$

and

$$\dot{\varepsilon}_{ij} = \bar{\dot{\varepsilon}}_{ij} + \tilde{\dot{\varepsilon}}_{ij}$$

into the power law for the total flow,

$$\sigma_{ij} = 2\eta \dot{\varepsilon}_{ij} - p\delta_{ij} ,$$

and keeping the first-order terms in terms of $\tilde{\dot{\varepsilon}}_{ij} / \bar{\dot{\varepsilon}}_{ij}$ [*Smith*, 1977; *Fletcher and Hallet*, 1983]:

$$\tilde{\sigma}_{xz} = 2\eta \tilde{\dot{\varepsilon}}_{xz} , \quad (6a)$$

$$\tilde{\sigma}_{xx} = \frac{2\eta}{n}\tilde{\dot{\varepsilon}}_{xx} - \tilde{p} , \quad (6b)$$

$$\tilde{\sigma}_{zz} = \frac{2\eta}{n}\tilde{\dot{\varepsilon}}_{zz} - \tilde{p} , \quad (6c)$$

where η is the effective viscosity for the basic flow and $\tilde{\sigma}_{xx}$, $\tilde{\sigma}_{xz}$, $\tilde{\sigma}_{zz}$, and $\tilde{p}$ are the stress components and pressure for the perturbed flow. The relationships in (6) are well known for introducing anisotropy in the perturbed flow when deformation follows a power law (that is, $n \neq 1$) [*Smith*, 1977]. The strain rate tensor for the perturbed flow is

$$\tilde{\dot{\varepsilon}}_{ij} = \begin{pmatrix} \tilde{\dot{\varepsilon}}_{xx} & \tilde{\dot{\varepsilon}}_{xz} \\ \tilde{\dot{\varepsilon}}_{zx} & \tilde{\dot{\varepsilon}}_{zz} \end{pmatrix} = \begin{pmatrix} \frac{\partial \tilde{u}}{\partial x} & \frac{1}{2}\left(\frac{\partial \tilde{u}}{\partial z} + \frac{\partial \tilde{w}}{\partial x}\right) \\ \frac{1}{2}\left(\frac{\partial \tilde{u}}{\partial z} + \frac{\partial \tilde{w}}{\partial x}\right) & \frac{\partial \tilde{w}}{\partial z} \end{pmatrix} . \quad (7)$$

Note that although the strain rate field for the basic flow is homogeneous, this is not the case for the perturbed flow. The primary concern in the instability analysis is to determine the strain and stress distribution and their evolution. The condition of incompressibility for the perturbed flow requires that

$$\tilde{\dot{\varepsilon}}_{xx} + \tilde{\dot{\varepsilon}}_{yy} = \frac{\partial \tilde{u}}{\partial x} + \frac{\partial \tilde{w}}{\partial z} = 0 . \quad (8)$$

This condition suggests the existence of a stream function that can be related to the velocity components by

$$\tilde{u} = \frac{\partial \tilde{\psi}}{\partial y} , \quad \tilde{w} = -\frac{\partial \tilde{\psi}}{\partial x} . \quad (9)$$

The stress components for the perturbed flow satisfy the stress equilibrium equations

$$\frac{\partial \tilde{\sigma}_{xx}}{\partial x} + \frac{\partial \tilde{\sigma}_{xz}}{\partial z} + X = 0 , \quad (10a)$$

$$\frac{\partial \tilde{\sigma}_{xz}}{\partial x} + \frac{\partial \tilde{\sigma}_{zz}}{\partial z} + Z = 0 , \quad (10b)$$

where X and Z are the body force components in the x and z directions. Substituting (7)-(9) into (10) and noting that $X = -(\partial V/\partial x)$ and $Z = -(\partial V/\partial z)$, where $V = -\rho g z$ is the gravitational potential, we obtain the following equation expressed in terms of the stream function:

$$\frac{\partial^4 \tilde{\psi}}{\partial x^4} + 2(2n-1)\frac{\partial^4 \tilde{\psi}}{\partial x^2 \partial z^2} + \frac{\partial^4 \tilde{\psi}}{\partial x^4} = 0 . \quad (11)$$

The general solution of this equation may be expressed by the following form [*Smith*, 1977]:

$$\tilde{\psi}(x,z) = \tilde{\phi}(z)\exp(i\alpha x), \quad (12)$$

where α is a real number to warrant a periodical solution in the x direction. The general solution for $\tilde{\phi}(z)$ satisfies the following equation [*Bassi and Bonnin*, 1988],

$$\begin{aligned} \tilde{\phi}(z) &= A_1 \cos\beta_1\lambda z \cosh\alpha_1\lambda z \\ &+ \frac{A_2 \sin\beta_1\lambda z}{\beta_1\lambda}\cosh\alpha_1\lambda_1 z \\ &+ A_3 \frac{\sin\beta_1\lambda z}{\alpha_1\beta_1\lambda^2}\sinh\alpha_1\lambda z \\ &- B_4 \frac{3}{\alpha_1\lambda^3}\left[\cos\beta_1\lambda z \sinh\alpha_a\lambda z - \frac{\alpha_1}{\beta_1}\sin\beta_1\lambda z \cosh\alpha_1\lambda z\right], \end{aligned} \quad (13)$$

where $\alpha_1 = n^{-1/2}, \beta_1 = (1-1/n)^{1/2}$. Once $\tilde{\phi}(z)$ is known, the general solutions for the velocity and stress components in the perturbed state can be derived from (6), (7), (12), and (13), respectively. The stress and velocity components for the per-

turbed flow satisfy the following relations at the interface:

$$\tilde{u}_i(x,z_i)=\tilde{u}_{i+1}(x,z_i), \tag{14}$$

$$\tilde{w}_i(x,z_i)=\tilde{w}_{i+1}(x,z_i), \tag{15}$$

$$\tilde{\sigma}_{xz}(x,z_i)-\tilde{\sigma}_{xz}(x,z_{i+1})= \tag{16}$$
$$4\dot{\bar{\varepsilon}}_{xx}(\frac{dh_i}{dx})[\eta_i(z_i)-\eta_{i+1}(z_{i+1})],$$

$$\tilde{\sigma}_{xz}(x,z_i)-\tilde{\sigma}_{xz}(x,z_{i+1})= \tag{17}$$
$$(\rho_{i+1}-\rho_i)gh_i(x),$$

where $h_i(x)$ is the topography at the ith interface, i = 1, 2, 3, and ρ_i is the density for the ith layer. Note that (14) to (17) show that the velocity is continuous for the perturbed flow across the interfaces but the stress components are discontinuous across the boundaries, producing a pressure jump that drives the instability [*Smith*, 1975].

If the vertical irregularity at an interface is a sinusoidal function of x such as $h(x,t)=h_{i0}(t)\sin(\lambda x)$, then the total growth rate of its amplitude may be expressed as the sum of vertical deformation rate due to both the basic flow and the perturbed flow [*Fletcher and Hallet*, 1983],

$$\frac{\partial h_{i0}(t)}{\partial t}=\dot{\bar{\varepsilon}}_{yy}h_{i0}+\tilde{w}(0,z_i). \tag{18}$$

If we further define a growth rate factor as [*Smith*, 1977; *Fletcher and Hallet*, 1983]

$$q_i-1=(1/\dot{\bar{\varepsilon}}_{xx})\frac{1}{h_{i0}}\frac{\partial h_{i0}}{\partial t}, \tag{19}$$

we can express amplitude of the sinusoidal interface as a function of time, such as

$$h_{i0}=C_0\exp[(q-1)\dot{\bar{\varepsilon}}_{xx}t], \tag{20}$$

where C_0 is an arbitrary constant. Because $\dot{\bar{\varepsilon}}_{xx}=-\dot{\bar{\varepsilon}}_{yy}$, as required by the incompressibility condition in (2), by comparing (18) and (19), we obtain

$$\frac{\partial h_{i0}(t)}{\partial t}=-\dot{\bar{\varepsilon}}_{xx}h_{i0}+\tilde{w}(0,z_i)=(q-1)\dot{\bar{\varepsilon}}_{xx}h_{i0}, \tag{21}$$

which can be further simplified to

$$\tilde{w}(0,z_i)-q\dot{\bar{\varepsilon}}_{xx}h_{i0}=0. \tag{22}$$

Equation (22) and boundary conditions of (14) to (17) at three interfaces and at $z=+\infty$ yield a system of 18 linear algebra equations with 18 unknown constants to be determined. These equations define the following dimensionless parameters [*Zuber et al.*, 1986]:

$$\begin{aligned} S_1&=(\rho_1-\rho_0)gz_1/\tau_1,\\ S_2&=(\rho_2-\rho_1)gz_1/\tau_2,\\ S_3&=(\rho_3-\rho_2)gz_1/\tau_3,\\ S_4&=(\rho_4-\rho_3)gz_1/\tau_4, \end{aligned} \tag{23a}$$

$$\begin{aligned} R_1&=\tau_1/\tau_2,\\ R_2&=\tau_1/\tau_3,\\ R_3&=\tau_1/\tau_4, \end{aligned} \tag{23b}$$

where $\tau_i=2\eta_i\dot{\bar{\varepsilon}}_{xx}$, i = 1, 2, 3, 4, is the average yield strength of each mechanical layer. Finally, the growth factor, q, is solved from the system of linear equations (14)-(17) and (22) as a function of the dimensionless parameters listed above, the thickness of each mechanical layers (z_i), and the dimensionless wave number, k'. That is,

$$q=q(S_1,S_2,S_3,S_4,R_1,R_2,R_3,z_1,z_2,z_3,k'), \tag{24}$$

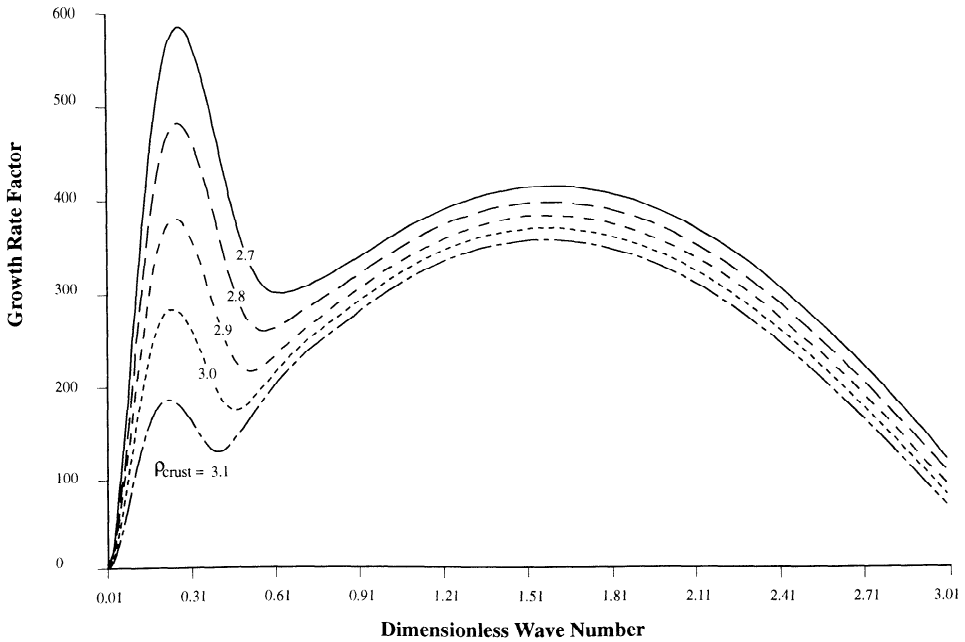

Figure 5. Relationship between the growth rate factor and the dimensionless wave number as a function of the crustal density (ρ_{crust}), which varies from 2.7 to 3.1 g cm^{-3}. Parameters used in the model are z_1= 10 km, z_2 = 60 km, z_3 = 40 km, R_1 = 100, R_2 = 0.5, R_3 = 50, τ_1 = 246 MPa, ρ_{mantle} = 3.2 g cm^{-3}. See text for discussion.

where $k' = 2\pi z_1 / \lambda$, and λ is the wavelength. In the following calculation a uniform density for the crust and the mantle is assumed (i.e., $\rho_1 = \rho_2 = \rho_{crust}$, $\rho_3 = \rho_4 = \rho_{mantle}$; $S_2 = S_4 = 0$). To approximate the plastic behavior of the upper crust and the mantle lithosphere, $n_1 = n_3 = 10^4$ are used. For the lower crust and the asthenosphere, $n_2 = n_4 = 3$ are selected. The horizontal strain rate is assumed to be 10^{-15} s^{-1}, a typical value for intracontinental deformation [e.g., *Brace and Kohlstedt*, 1980].

5.2. Results

Figure 5 shows the relationship between the growth rate factor and the dimensionless wave number as a function of crustal density. The parameters used in the model are $z_1 = 10$ km, $z_2 = 60$ km, $z_3 = 40$ km, $R_1 = 100$, $R_2 = 0.5$, $R_3 = 50$, $\tau_1 = 246$ MPa, $\rho_{mantle} = 3.2$ g cm^{-3}. Selecting $R_1 = 100$ implies that the upper crust is 2 orders of magnitude stronger than the lower crust, and $R_2 = 0.5$ implies that the plastic mantle lithosphere is a factor of 5 stronger than the plastic upper crust. Finally, $R_3 = 50$ implies that the upper crust is 50 times stronger than the asthenosphere. This figure shows that for a given density contrast between the crust and the mantle, the growth rate factor has two maximums: one corresponds to a higher wave number and the other corresponds to a lower wave number. As demonstrated by *Zuber et al.* [1986], the peak corresponding to the lower wave number is controlled by the presence of a strong upper mantle, whereas the peak corresponding to the higher wave number is controlled by the presence of a strong upper crust. When the value of one peak is greater than the other, extensional instability is dominated by the wave number related to the larger peak, which in turn decides the dominant wave length and therefore the spacing of extensional instability.

When the crustal density is between 3.1 and <~2.92 g cm^{-3}, the peak value for the growth factor corresponding to the high wave number is greater than that corresponding to the lower wave number (Figure 5). This implies that the spacing of extensional instability is dominated at a wave number of $k' \approx 1.56$ or a wave length $L \approx 40$ km. However, as the density of the crust decreases, the peak value of the growth factor corresponding to the lower wave number increases faster than that corresponding to the higher wave number. When the crustal density is equal to ~2.92 g cm^{-3}, the two peak values are nearly equal. Under this condition, the extensional instability is dominated by two different wave numbers ($k'_{high} \approx 0.25$, $k'_{low} \approx 1.56$) expressed by two different dominant wavelengths ($L_{long} \approx 251$ km, $L_{short} \approx 40$ km). When the crustal density is <~2.92 g cm^{-3}, the peak value correlated with the lower wave number exceeds that correlated with the higher wave number. Thus, with all other conditions held the same, the dominant wave number of the instability switches from $k' \approx 1.56$ when the crustal density is between 3.10 g cm^{-3} and 2.92 g cm^{-3} to $k' \approx 0.25$-0.30 when the crustal density is between 2.92 g cm^{-3} and 2.70 g cm^{-3}. The latter wave numbers of $k' \approx 0.25$-0.30 correspond to dominant wavelengths of $L \approx 210$-250 km. This result implies that a subtle change in crustal density from slightly below 2.92 g cm^{-3} to slightly above 2.92 g cm^{-3} would cause a change in the spacing of extensional instability.

The role of relative strength contrast between the upper crust (τ_1) and the mantle lithosphere (τ_3) in controlling the dominant wavelength for the initiation of extensional instability is shown in Figure 6. In this case, I used the following parameters: $z_1 = 10$ km, $z_2 = 60$ km, $z_3 = 40$ km, $R_1 = 100$, $R_3 = 50$, $\tau_3 = 246$ MPa, $\rho_{mantle} = 3.20$ g cm^{-3}, $\rho_{crust} = 2.95$ g cm^{-3}, and R_2 varies from 1 to 5. As the strength of the upper crust increases, the peak value of the growth rate factor corresponding to the higher wave number increases much faster than that corresponding to the lower wave number. This implies that if the strength of the upper crust is significantly greater than that of the upper mantle, the short-wavelength instability ($k' \approx 1.3$-1.5 or $L \approx 41$-48 km) prevails. It also shows that the high wave number peak corresponds to the presence of the strong upper crust.

The role of the upper and lower crustal thickness in controlling the dominant wavelength of extensional instability is shown in Figures 7 and 8, respectively. In Figure 7, I assume that $z_2 = 60$ km, $z_3 = 40$ km, $R_1 = 100$, $R_2 = 0.5$, $R_3 = 50$, $\tau_1 = 246$

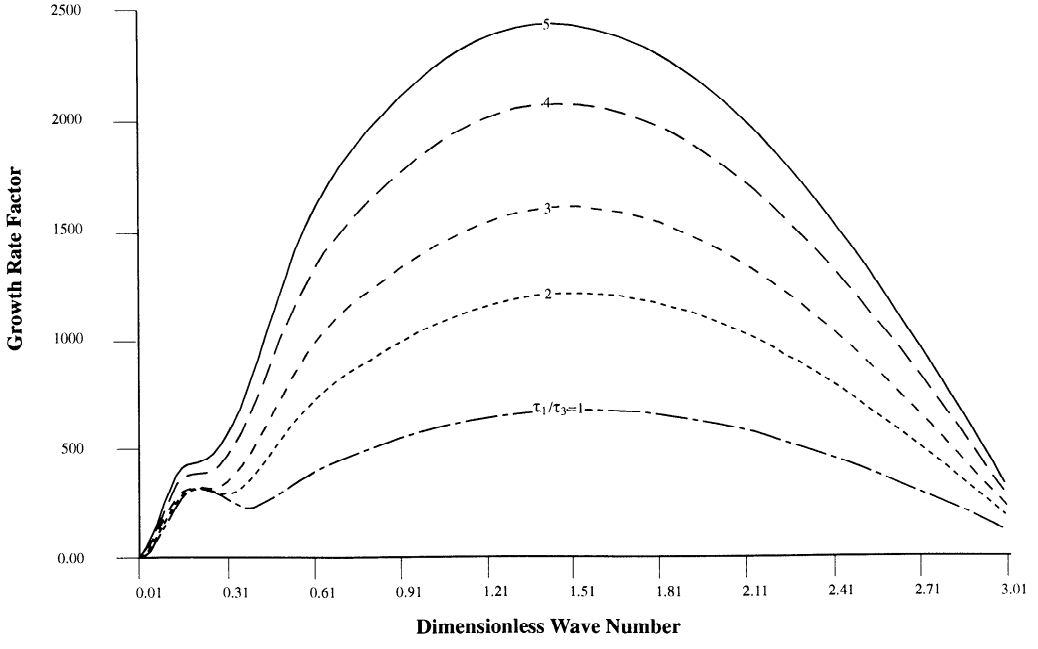

Figure 6. Relationship between the growth rate factor and the dimensionless wave number as a function of strength contrast ($R_2 = \tau_1/\tau_3$) of the upper crust (τ_1) and the mantle lithosphere (τ_3): $z_1 = 10$ km, $z_2 = 60$ km, $z_3 = 40$ km, $R_1 = 100$, $R_3 = 50$, $\tau_3 = 246$ MPa, $\rho_{mantle} = 3.20$ g cm^{-3}, and $\rho_{crust} = 2.95$ g cm^{-3}. Note that as the strength of the upper crust increases, the peak value of the growth rate factor corresponding to the higher wave number increases much faster than that corresponding to the lower wave number.

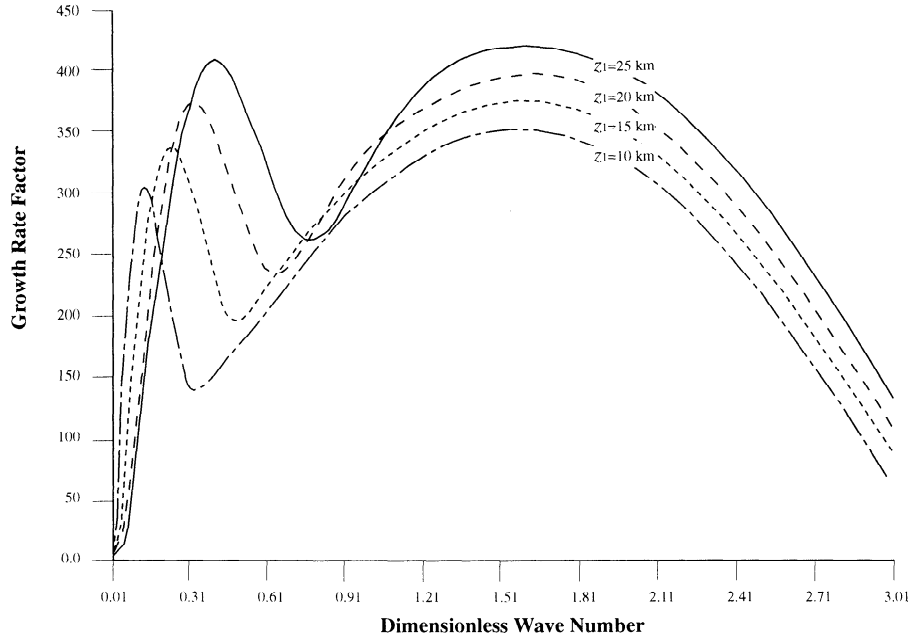

Figure 7. Relationship between the growth rate factor and the dimensionless wave number as a function of the upper crustal thickness (z_1): z_2 = 60 km, z_3 = 40 km, R_1 = 100, R_2 = 0.5, R_3 = 50, τ_1 = 246 MPa, ρ_{mantle} = 3.20 g cm^{-3}, and ρ_{crust} = 2.95 g cm^{-3}, with z_1 varying from 5 to 20 km. Note that a change in the thickness of the upper crust does not switch the dominant wave number from one peak to the other, although the wave number corresponding to each peak changes systematically as the crustal thickness varies.

MPa, ρ_{mantle} = 3.20 g cm^{-3}, and ρ_{crust} = 2.95 g cm^{-3}, with z_1 varying from 10 to 25 km. In this case, a change in the thickness of the upper crust does not switch the dominant wave number from one peak of the growth rate curve to the other, although the wave number corresponding to each peak changes slightly as the crustal thickness increases (Figure 7). The amplitude of the lower wave number peaks increases as the upper crustal thickness increases, whereas the amplitude of the higher wave number peaks also increases as the upper crustal thickness increases. For the low wave number peaks their corresponding wave numbers increase from ~0.16 to ~0.41 as the upper crustal thickness increases. This corresponds to an increase in the wavelength of extensional instability from ~190 km to ~300 km. For the high wave number peaks the wave numbers

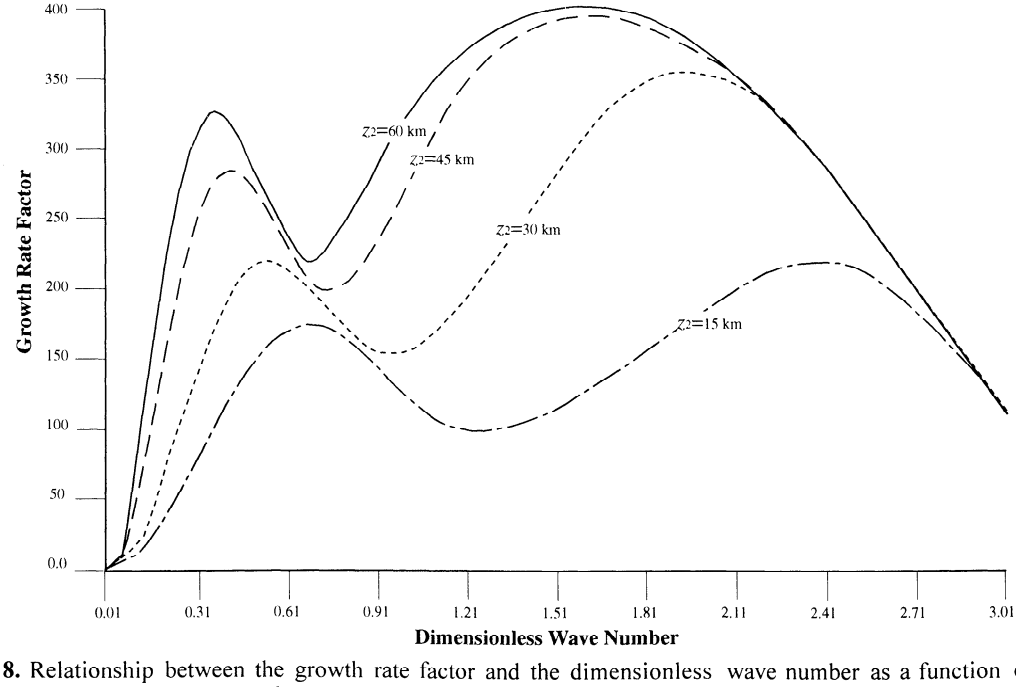

Figure 8. Relationship between the growth rate factor and the dimensionless wave number as a function of the lower crustal thickness (z_3): z_1 = 15 km, z_3 = 40 km, R_1 = 100, R_2 = 0.5, R_3 = 50, τ_1 = 246 MPa, ρ_{mantle} = 3.20 g cm^{-3}, and ρ_{crust} = 2.95 g cm^{-3}, with z_2 varying from 15 to 60 km. Similar to the case shown in Figure 7, there is no switch in the dominant wave number as a result of an increase in the thickness of the lower crust. However, wave number corresponding to each peak changes systematically as the thickness of the lower crust varies.

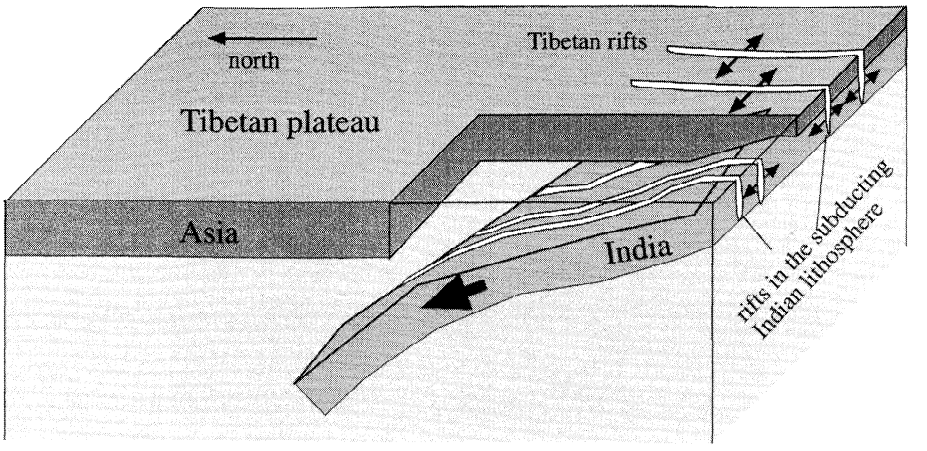

(a)

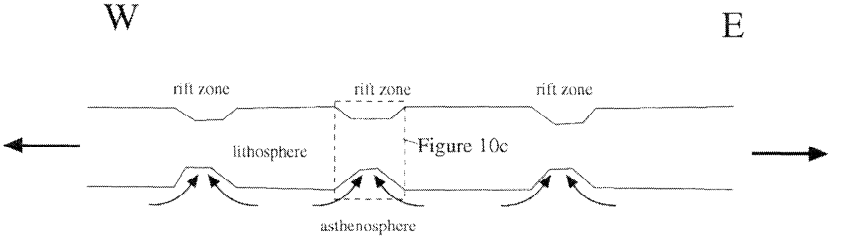

(b)

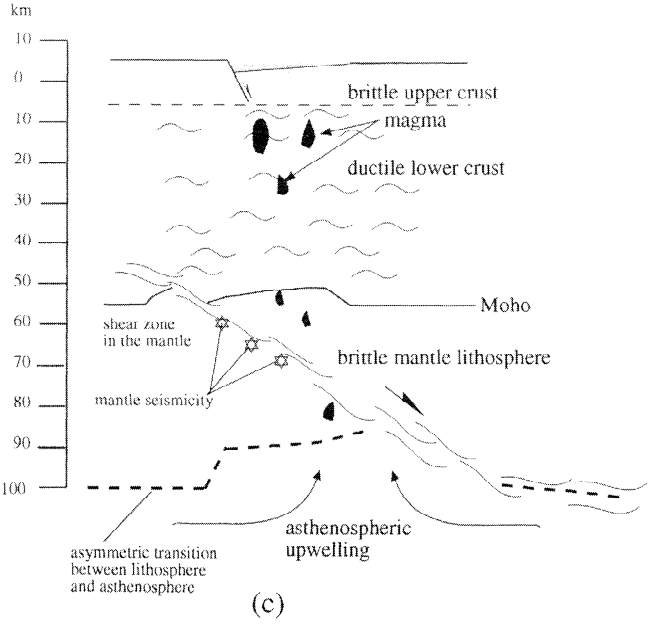

(c)

Figure 9. (a) A schematic diagram showing Indian mantle lithosphere directly beneath The Himalaya is involved in east-west extension. (b) A schematic diagram showing possible mode of Cenozoic lithospheric extension in Asia including Tibet. (c) A detailed cross section showing possible structural relationships within each rift zone. Upper crustal normal faults sole into the ductile shear zones in the middle and the lower crust. The mantle lithosphere is thinned in response to extension by either brittle faulting or ductile flow. The thinning of the mantle lithosphere is responsible for upwelling of the mantle asthenosphere, which in turn could have produced synrifting magmatism such as those observed in the rift valley of the Shanxi graben [*Wang et al.*, 1996].

corresponding to the peak values decrease slightly from ~1.6 to ~1.5.

In Figure 8, I assume that z_1 = 15 km, z_3 = 40 km, R_1 = 100, R_2 = 0.5, R_3 = 50, τ_1 = 246 MPa, ρ_{mantle} = 3.20 g cm^{-3}, and ρ_{crust} = 2.95 g cm^{-3}, with z_2 varying from 15 to 60 km. Similar to the case shown in Figure 7, there is no switch in the dominant wave number as a result of an increase in the thickness of the lower crust. However, wave number corresponding to each peak changes systematically as the thickness of the lower crust increases. For both peaks in Figure 8, wave numbers decrease when crustal thickness increases. For the low wave number peak its maximum value corresponds to a variation in rift spacing from ~145 km for a 15-km-thick lower crust to ~285 km for a 60-km-thick lower crust.

6. Discussion

The above analysis shows that when the crustal density is greater than ~2.90 g cm^{-3}, with a 10-km upper crust and 60-km lower crust, the short-wavelength instability is favored. However, when the crustal density is <~2.90 g cm^{-3}, the long-wavelength instability prevails. This mechanism may help understand the origin of a bimodal distribution of rift spacing in south Tibet. Underthrusting of Indian continent beneath Asia [*Powell and Conaghan*, 1973; *Owens and Zandt*, 1997] may have added its Late Proterozoic-Mesozoic sediments into the Tibetan crust, which would have lowered the overall crustal density of Tibet to favor the development of an extensional instability at longer wavelengths. This implies that the closely spaced short rifts in south central part of south Tibet occurred first, which was followed by the formation of widely spaced long rifts.

Once the choice of long- or short-wavelength instability is determined, the rift spacing is most sensitive to the lower crustal thickness: a thicker lower crust favors a wider rift spacing, whereas a thinner lower crust favors a shorter rift spacing. This may qualitatively explain the systematic decrease in rift spacing from south to north between The Himalaya and central Tibet (Figure 3), as its thickness decreases northward from 80-85 km in The Himalaya to ~75 km in southern Tibet to ~55 km in central Tibet [*Hirn et al.*, 1984; *Zhao and Xie*, 1993; *Nelson et al.*, 1996; *Owens and Zandt*, 1997].

As shown by *Zuber et al.* [1986], the mode of extensional instability corresponding to wavelengths of 200-250 km on the growth rate factor plots, such as those shown in Figures 5-8, could be related to the presence and involvement of the mantle lithosphere. If their conjecture applies to the case in Tibet, it means that wavelengths of 150-300 km for rift spacing in both The Himalaya and Tibet reflect the involvement of the mantle lithosphere during Cenozoic east-west extension. It also implies that the mantle lithosphere directly beneath The Himalaya, which is part of the Indian plate, must have also been extended together with its upper crustal rifts (Figure 9a). Extension of the mantle lithosphere beneath The Himalaya is consistent with deep earthquakes whose epicenters are at the depths between 80 and 100 km in the region [*Chen and Kao*, 1996]. Because the Indian mantle lithosphere is involved in extension, oblique subduction of India can be ruled out as the sole cause for the east-west Tibetan extension [*McCaffrey and Nabelek*, 1998]. This leads to two possibilities: (1) the extension was induced by east-west stretching of the entire lithosphere in the Himalaya and Tibet (passive rifting), and (2) extension was induced by mantle flow in the asthenosphere (active rifting). To definitively resolve these questions is clearly beyond the scope of this paper. However, a comparison of igneous activity, age of onset of rifting, and style of deformation between Tibetan rifts and Cenozoic rifts in north China and Siberia may provide some insights.

Postcollision volcanism in Tibet began at ~40 Ma [*Chung et al.*, 1998; *Deng*, 1998]. However, rifting did not initiate until ~8-4 Ma [*Harrison et al.*, 1995; *Yin et al.*, 1999]. This history is similar to the igneous activity in the Lake Baikal region, where initial volcanism occurred at ~29 Ma [*Kiselev*, 1987; *Delvaux et al.*, 1997], but rift did not develop until about 8 Ma [*Delvaux et al.*, 1997]. This history is also similar to the Shanxi graben and its adjacent regions, which experienced extensive basaltic eruption (i.e., the Fanshi Basalt) at about 30-23 Ma [*Wang*, 1982] (Figure 1). However, the graben did not begin to develop at ~6 Ma [*Wang et al.*, 1996].

The mode of extension is similar among the Tibetan, Baikal, and Shanxi rifts, all involve mantle lithosphere as depicted in Figure 9. Modeling of gravity data, detailed analysis of teleseismic travel times, and the occurrence of seismicity at a depth of 40-50 km in the upper mantle suggest that the mantle lithosphere is involved during the formation of the Baikal rift [e.g., *Rupple et al.*, 1993; *van der Beek*, 1997; *Gao et al.*, 1994; *Deverchere et al.*, 1991]. The presence of extensive Quaternary basaltic eruption centers along the Shanxi graben [*Wang et al.*, 1996] also implies that extension of the Shanxi graben is deep-seated, involving the mantle lithosphere.

The broad similarities in the history of volcanism (i.e., it occurred some 10-30 Myr prior to rifting), the age of rift initiation (8-4 Ma), extension involving mantle lithosphere, and the trend (north-south) and the direction of extension (east-west) suggest that rifts in Tibet and those in north China and southeast Siberia may have shared the same origin. It implies that gravitational collapse [e.g., *Dewey*, 1988] or convective removal of the mantle lithosphere beneath Tibet [*England and Houseman*, 1989] cannot be the only causes for the development of Tibetan rifts. Instead, this would require a boundary condition at a scale of thousands of kilometers applied for entire east Asia. One possibility is that eastern Asia had experienced mantle upwelling induced by subduction of the Pacific plate beginning at ~40-35 Ma [*Northrup et al.*, 1995]. This process caused thermal weakening of the lithosphere and eventual rifting in Asia at ~8-4 Ma. This may explain why initiation of post-Indo-Asian collision volcanism predates rifting in Tibet, Lake Baikal, and Shanxi.

7. Conclusions

Rift spacing in the Himalaya and Tibet decreases systematically from south to north. In The Himalaya south of the Indus-Yalu suture, it is 191±67 km. In south Tibet between the Indus-Yalu suture and the Bangong-Nujiang suture, it is 146±34 km. Farther to the north in central Tibet between the Bangong-Nujiang suture and the Jinsha suture, it is 101±31 km. Instability analysis suggests that widely spaced rifts in The Himalaya and Tibet may have been related to the presence of a relatively light crust (crustal density <~2.90 g cm^{-3}) and a strong mantle lithosphere (more than a factor of 5 stronger than the upper crust) throughout Tibet, and its systematic decrease in rift spacing may be explained by the northward decrease in crustal thickness in Tibet. Regional synthesis suggests that the mode of east-west extension in Tibet is similar to that for the Baikal rift and Shanxi graben in southeast Siberia and north China, all involving the mantle lithosphere during east-west extension and starting to develop at about the same time between 8 and 4 Ma. This would require a boundary condition at a scale of thousands of kilometers applied in east Asia for their initiation and subsequent development. One possibility is that entire eastern Asia had experienced mantle upwelling beginning at ~40-35 Ma. This process caused thermal weakening of the lithosphere and eventual rift development at ~8-4 Ma. This may explain why initiation of post-Indo-Asian collision volcanism predates rifting in Tibet, Lake Baikal, and Shanxi regions.

Acknowledgments. I thank X. Kong for writing a computer code to solve the eigenvalue problem in the instability analysis, Mian Liu for sharing his thoughts through unpublished manuscripts on the dynamics of the Tibetan plateau and extension in eastern Asia, and Mark Harrison and Paul Tackley for enlightening my thoughts on the origin of Asian rifts. Comments by Eric Cowgill, Paul Kapp, and Mike Taylor on a preliminary draft have improved the clarity of the paper. Doug Nelson, Mian Liu, and Peter Bird critically reviewed the manuscript and provided many constructive suggestions. I m grateful to Michael Taylor, who prepared Plate 1a for this study. This work is supported by the US National Science Foundation and by Lawrence Livermore National Laboratory, grant 99-GS005, awarded to F. J. Ryerson and A. Yin.

References

Allegre, C. J., et al., Structure and evolution of the Himalaya-Tibet orogenic belt, *Nature, 307*, 17-22, 1984.

Armijo, R., P. Tapponnier, J. P. Mercier, and T. Han, Quaternary extension in southern Tibet, *J. Geophys. Res., 91*, 13,803-13,872, 1986.

Armijo, R., P. Tapponnier, and T. Han, Late Cenozoic right-lateral strike-slip faulting across southern Tibet, *J. Geophys. Res., 94*, 2787-2838, 1989.

Bassi, G., and J. Bonnin, Rheological modeling and deformation instability of lithosphere under extension, *Geophys. J., 93*, 485-504, 1988.

Benes, V., and P. Davy, Modes of continental lithospheric extension: Experimental verification of strain localization processes, *Tectonophysics, 254*, 69-87, 1996.

Biot, M. A., Theory of folding of stratified viscoelastic media and its implications in tectonics and orogenesis, *Geol. Soc. Am. Bull. 72*, 1595-1620, 1961.

Bird, P., Lateral extrusion of lower crust from under high topography in the isostatic limit, *J. Geophys. Res., 96*, 10,275-10,286, 1991.

Blisniuk, P. M., B. Siwen, O. Kuchel, and L. Ratschbacher, Late Neogene extension in the Shuang Hu graben, central Tibet, *Eos Trans. AGU, 79 (45)*, Fall Meet. Suppl., F794, 1998.

Brace, W.F., and D. L. Kohlstedt, Limits on lithospheric stress imposed by laboratory experiments, *J. Geophys. Res., 85*, 6248-6252, 1980.

Burchfiel, B. C., Q. Deng, P. Molnar, L. H. Royden, Y. Wang, P. Zhang, and W. Zhang, Intracrustal detachment with zones of continental deformation, *Geology, 17*, 748-752, 1989.

Burchfiel, B. C., Z. Chen, L. H. Royden, Y. Liu, and C. Deng, Extensional development of Gabo valley, southern Tibet, *Tectonophysics, 194*, 187-193, 1991.

Chapple, W. M., A mechanical theory of finite-amplitude rock folding, *Geol. Soc. Am. Bull., 79*, 47-68, 1968.

Chen, W. P., and H. Kao, Seismotectonics of Asia: Some recent progress, in *The Tectonics of Asia*, edited by A. Yin and T. M. Harrison, pp. 37-52, Cambridge Univ. Press, New York, 1996.

Chen, W. P., and P. Molnar, Focal depths of intracontinental and intraplate earthquakes and their implications for the thermal and mechanical properties of the lithosphere, *J. Geophys. Res., 88*, 4183-4214, 1983.

Chung, S. L., C. C. Lo, T. Y. Lee, Y. Zhang, Y. Xie, X. Li, K. L. Wang, and P. L. Wang, Diachronous uplift of the Tibetan plateau starting 40 Myr ago, *Nature, 394*, 769-773, 1998.

Cogan, M. J., K. D. Nelson, W. S. F. Kidd, C. Wu, and Project INDEPTH Team, Shallow structure of the Yadong-Gulu rift, southern Tibet, from refraction analysis of Project INDEPTH common midpoint data, *Tectonics, 17*, 46-61, 1998.

Coleman, M., and K. Hodges, Evidence for Tibetan plateau uplift before 14 Myr ago from a new minimum estimate for east-west extension, *Nature, 374*, 49-52, 1995.

Delvaux, D., R. Moeys, G. Stapel, C. Petit, K. Levi, A. Miroshnichenko, V. Ruzhich, and V. San'kov, Paleostress reconstructions and geodynamics of the Baikal region, Central Asia, part 2, Cenozoic rifting, *Tectonophysics, 282*, 1-38, 1997.

Deng, W., *Cenozoic Intraplate Volcanic Rocks in the Northern Qinghai-Xizang Plateau* (in Chinese with English abstract), 180 pp., Geologic Publ. House, Beijing, 1998.

Deverchere, J., F. Houdry, and M. Diament, Evidence for seismogenic upper mantle and lower crust in the Baikal rift, *Geophys. Res. Lett., 18*, 1099-1102, 1991.

Dewey, J. F., Extensional collapse of orogens, *Tectonics, 7*, 1123-1140, 1988.

Dewey, J. F., R. M. Shackleton, Chang C., and Sun Y., The tectonic evolution of the Tibetan Plateau, *Philos. Trans. R. Soc. London, Ser. A, 327*, 379-413, 1988.

England, P. and G. Houseman, Finite strain calculations of continental deformation, 2, Comparison with the India-Asia collision zone, *J. Geophys. Res., 91*, 3664-3676, 1986.

England, P., and G. Houseman, Extension during continental convergence, with application to the Tibetan Plateau, *J. Geophys. Res., 94*, 17561-17579, 1989.

Fielding, E. J., B. L. Isacks, M. Barazangi, and C.C. Duncan, How flat is Tibet, *Geology, 22*, 163-167, 1994.

Fletcher, R. C., Wavelength selection in the folding of a single layer with power-law rheology, *Am. J. Sci., 274*, 1029-1043, 1974.

Fletcher, R. C., and B. Hallet, Unstable extension of the continental lithosphere: A mechanical model for Basin-and-Range structure, *J. Geophys. Res., 88*, 7457-7466, 1983.

Gao, S., P. M. Davis, H. Liu, P. D. Slack, Y. A. Zorin, N. A. Logatchev, M. Kogan, P. D. Burkholder, and R. P. Meyer, Asymmetric upward of the asthenosphere beneath the Baikal rift zone, Siberia, *J. Geophys. Res., 99*, 15,319-15,330, 1994.

Harrison, T. M., P. Copeland, W. S. F. Kidd, and A. Yin, Raising Tibet, *Science, 255*, 1663-1670, 1992.

Harrison, T. M., P. Copeland, W. S. F. Kidd, and O. Lovera, Activation of the Nyainqentanghla shear zone: Implications for uplift of the southern Tibetan Plateau, *Tectonics, 14*, 658-676, 1995.

Hauck, M. L., K. D. Nelson, L. D. Brown, W. J. Zhao, and A. R. Ross, Crustal structure of the Himalayan orogen at similar to 90° east longitude from Project INDEPTH deep reflection profiles, *Tectonics, 17*, 481-500, 1998.

Hirn, A., et al., Crustal structure and variability of the Himalayan border of Tibet, *Nature, 307*, 23-25, 1984, 1984.

Holt, W. E., Correlated crust and mantle strain fields in Tibet, *Geology, 28*, 67-70, 2000.

Kapp, P., A. Yin, M. A. Murphy, T. M. Harrison, and F. J. Ryerson, Discovery of a major blueschist-bearing detachment fault system in the Shuang Hu region of the Qiangtang block, northern Tibet, *Geol. Soc. Am. Abstr. Programs, 29*, 144, 1997.

Kapp, P., A. Yin, C. E. Manning, M. Murphy, T. M. Harrison, M. Spurlin, Din L., and Deng X., Post-mid-Cretaceous shortening along the Banggong-Nujiang suture and in west-central Qiangtang, Tibet, *Eos Trans. AGU, 79 (45)*, Fall Meet. Suppl., F794, 1998.

Kiselev, A. I., Volcanism of the Baikal rift zone, *Tectonophysics, 143*, 235-244, 1987.

Klootwijk, C. T., P. J. Conaghan, C. M. and Powell. The Himalayan arc: Large-scale continental subduction, oroclinal bending, and back-arc spreading, *Earth Planet. Sci. Lett., 75*, 316-319, 1985.

Lee, T.-Y., C. Lo, S. Chung, C. Chen, P. Wang, W. Lin, N. Hoang, C. T. Chi, and N. T. Yem, $^{40}Ar/^{39}Ar$ dating result of Neogene basalt in Vietnam and its tectonic implication, in *Mantle Dynamics and Plate Interactions in East Asia, Geodyn. Ser.*, vol. 27, edited by M. F. J. Flower et al., pp. 317-330, AGU, Washington, D. C., 1998.

Liao, K. (ed.), *Atlas of the Qinghai-Xizang Plateau*, 237 pp., Inst. of Geogr., Sci. Publ. House, Beijing, 1990.

Mancktelow, N. S., and M. Abbassi, Single layer buckle folding in nonlinear materials, II, Comparison between theory and experiment, *J. Struc. Geol., 14*, 105-120, 1992.

Martinod, J., and P. Davy, Periodic instabilities during compression of the lithosphere, 1, Deformation modes from an analytic perturbation method, *J. Geophys. Res., 97*, 1999-2014, 1992.

Martinod, J., and P. Davy, Periodic instabilities during compression of the lithosphere, 2, Analogue experiments, *J. Geophys. Res., 99*, 12,057-12,069, 1994.

Masek, J. G, B. L. Isacks, E. J. Fielding, and J. Browaeys, Rift flank uplift in Tibet: Evidence for a viscous lower crust, *Tectonics, 13*, 659-667, 1994.

McCaffery, R., and J. Nabelek, Role of oblique convergence in the active deformation of the Himalayas and southern Tibet plateau, *Geology, 26*, 691-694, 1998.

Mercier, J.-L., R. Armijo, P. Tapponnier, E. Carey-Gailhardis, and T. L. Han, Change from Tertiary compression to Quaternary extension in southern Tibet during the India-Asia collision, *Tectonics, 6*, 275-304, 1987.

Molnar, P., and W. P. Chen, Focal depths and fault plane solution of earthquake under the Tibetan plateau, *J. Geophys. Res., 88*, 1180-1196, 1983.

Molnar, P., and H. Lyon-Caen, Fault plane solutions of earthquakes and active tectonics of the Tibetan plateau and its margins, Geophys. *J. Int., 99*, 123-153, 1989.

Molnar, P., and P. Tapponnier, Active tectonics of Tibet, *J. Geophys. Res., 83*, 5361-5375, 1978.

Molnar, P., P. England, and J. Martinod, Mantle dynamics, the uplift of the Tibetan Plateau, and the Indian monsoon, *Rev. Geophys., 31*, 357-396, 1993.

Murphy, M. A., A. Yin, T. M. Harrison, S. B. Durr, W. S. F. Kidd, Z. Chen, F. J. Ryerson, X. Wang, and X. Zhou, Significant crustal shortening in south-central Tibet prior to the Indo-Asian collision, *Geology, 25*, 719-722, 1997.

Nelson, K. D., et al., Partial molten middle crust beneath southern Tibet: Synthesis of Project INDEPTH results, *Science, 274*, 1684-1688, 1996

Ni, J., and J. York, Late Cenozoic tectonics of the Tibetan Plateau, *J. Geophys. Res., 83*, 5377-5384, 1978.

Northrup, C. J., L. H. Royden, and B. C. Burchfiel, Motion of the Pacific plate relative to Eurasia and its potential relation to Cenozoic extension along the eastern margin of Eurasia, *Geology, 23*, 719-722, 1995.

Owens, T. J., and G. Zandt, Implications of crustal property variation for models of Tibetan plateau evolution, *Nature, 387*, 37-43, 1997.

Pan G., Wang P., Xu Y., Jiao S., and Xiang T., *Cenozoic Tectonic Evolution of the Qinghai-Xiang Plateau*, Geologic Publ. House, Beijing, 1990.

Pan, Y., and W. S. F. Kidd, Nyainqentanghla shear zone: A late Miocene extensional detachment in the southern Tibetan Plateau, *Geology, 20*, 775-778, 1993.

Peltzer, G. P., P., Tapponnier, Z. Zhang, and Z. Q. Xu, Neogene and Quaternary faulting in and along the Qinling Shan, *Nature, 317*, 500-505, 1985.

Powell, C. M., and P. G. Conaghan, Plate tectonics and the Himalayas. *Earth Planet. Sci. Lett., 20*, 1-12, 1973.

Ratschbacher, L., W. Frisch, G. Liu, and C. Chen, Distributed deformation in southern and western Tibet during and after the India-Asia collision, *J. Geophys. Res., 99*, 19,917-19,945, 1994.

Ricard, Y., and C. Froidevaux, Stretching instabilities and lithospheric boundinage, *J. Geophys. Res.*, 91, 8314-8324, 1986.

Rothery, D. A., and S. A. Drury, The neotectonics of the Tibetan plateau, *Tectonics, 3*, 19-26, 1984.

Royden, L., Coupling and decoupling of crust and mantle in convergent orogens: Implications for strain partitioning in the crust, *J. Geophys. Res., 101*, 17,679-17,705, 1996.

Rupple, C., M. G. Kogan, and M. K. McNutt, Implications of new gravity data for Baikal rift zone structure, *Geophys. Res. Lett., 20*, 1635-1638, 1993.

Seeber, L., and J. G. Armbruster, Some elements of continental subduction along the Himalayan front, *Tectonophysics, 105*, 263-278, 1984.

Seeber, L., and A. Pecher, Strain partitioning along the Himalayan arc and the Nanga Parbat antiform, *Geology, 26*, 791-794, 1998.

Smith, R. B., Unified theory of the onset of folding, boundinage, and mullion structure, *Geol. Soc. Am. Bull., 86*, 1601-1609, 1975.

Smith, R. B., Formation of folds, boundinage, and mullions in non-Newtonian materials, *Geol Soc. Am Bull., 88*, 247-266, 1977.

Stewart, J. H., Basin and Range structure: A system of horsts and grabens produced by deep-seated extension, *Geol. Soc. Am. Bull., 82*, 1019-1043, 1971.

Tapponnier, P., and P. Molnar, Active faulting and tectonics of China, *J. Geophys. Res., 82*, 2905-2930, 1977.
Tapponnier, P., J. L. Mercier, R. Armijo, T. Han, and J. Zhao. Field evidence for active normal faulting in Tibet, *Nature, 294*, 410-414, 1981.
Tapponnier, P., G. Peltzer, A. Y. Le Dain, R. Armijo, and P. Cobbold, Propagating extrusion tectonics in Asia: New insights from simple experiments with plasticine, *Geology, 10*, 611-616, 1982.
Traynor, J. J., and C. Sladen, Tectonic and stratigraphic evolution of the Mongolian People's Republic and its influence on hydrocarbon geology and potential, *Mar. Petr. Geol., 12*, 35-52, 1995.
van der Beek, P., Flank uplift and topography at the central Baikal Rift (SE Siberia): A test of kinematic models for continental extension, *Tectonics, 16*, 122-136, 1997.
Wang, H. Z. (ed.), *Atlas of the Paleogeography of China*, 85 pp., Chin. Cartogr. Publ. House, Beijing, 1982.
Wang, N., J. Yang, Z. Xia, D. Me, Y. Li, and M. Pan, *Cenozoic Sedimentation and Tectonic Geomorphology of the Shanxi Graben*, 400 pp., Chin. Sci. Publ. House, Beijing, 1996.
Ye, H., B. Zhang, and F. Mao, The Cenozoic tectonic evolution of the great north China: Two types of rifting and crustal necking in the great north China and their tectonic implications, *Tectonphysics, 133*, 217-227, 1987.
Yin, A., and S. Nie, A Phanerozoic palinspastic reconstruction of China and its neighboring regions, in *The Tectonic Evolution of Asia*, edited by A. Yin and T. M. Harrison, pp. 442-485, Cambridge Univ. Press, New York, 1996.
Yin, A., and T.M. Harrison, Geologic evolution of the Himalayan-Tibetan orogen, *Annu. Rev. Earth Planet. Sci., 28*, 211-280, 2000.
Yin, A., T. M. Harrison, F. J. Ryerson, W. J. Chen, W. S. F. Kidd, and P. Copeland. Tertiary structural evolution of the Gangdese thrust system in southeastern Tibet, *J. Geophys. Res., 99*, 18,175-18,201, 1994.
Yin, A., P. Kapp, C. E. Manning, T. M. Harrison, Ding L., and Deng X., Extensive exposure of Mesozoic melange in Qiangtang and its role in the Cenozoic development of the Tibetan Plateau, *Eos Trans. AGU, 79 (45)*, Fall Meet. Suppl., F816, 1998.
Yin, A., Kapp, P., M. Murphy, C. E. Manning, T. M. Harrison, Ding L., Deng X., and Wu C., Significant late Neogene east-west extension in north Tibet, *Geology, 27*, 787-790, 1999.
Yu X., The Haoti alkaline ultrabasic volcanic rocks from Tanchang, Gansu province: A potassic ultramafic lamprophyre containing the upper mantle-derived xenoliths and megacrystals (in Chinese with English abstract), *Geol. Rev., 37*, 144-153, 1991.
Zhang, Y. Q., J. L. Mercier, and P. Vergely, Extension in the graben system around the Ordos (China), and its contribution to the extrusion tectonics of south China with respect to Gobi-Mongolia, *Tectonophysics, 285*, 41-75, 1998.
Zhao, L. S., and D. V. Helmberger, Geophysical implications from locations of Tibetan earthquakes: Hot lithosphere, *Geophys. Res. Lett., 18*, 2205-2208, 1991.
Zhao, L. S., and J. Xie, Lateral variations in compressional velocities beneath the Tibetan Plateau from *Pn* traveltime topography, *Geophys. J. Int., 115*, 1070-1084, 1993.
Zhao, W. L., and W. J. Morgan, Injection of Indian crust into Tibetan lower crust: A two-dimensional finite element model study, *Tectonics, 6*, 489-504, 1987.
Zhao, W., K. D. Nelson, and Project INDEPTH Team, Deep seismic reflection evidence for continental underthrusting beneath southern Tibet, *Nature, 366*, 557-559, 1993.
Zuber, M., and E. M. Pamentier, Finite amplitude of folding of a continuously viscosity-stratified lithosphere, *J. Geophys. Res., 101*, 5489-5498, 1996.
Zuber, M. T., E. M. Pamentier, and R. C. Fletcher, Extension of continental lithosphere: A model for two scales of Basin and Range deformation, *J. Geophys. Res., 91*, 4826-4838, 1986.

A. Yin, Department of Earth and Space Sciences, University of California, 3806 Geology Building, Los Angeles, CA 90095-1567. (yin@ess.ucla.edu)

(Received September 27, 1999; revised January 4, 2000; accepted May 3, 2000.)